Matter

CellPress

Article

In Situ Coupling of Colloidal Silica and Li Salt Anion toward Stable Li Anode for Long-Cycle-Life Li-O_2 Batteries

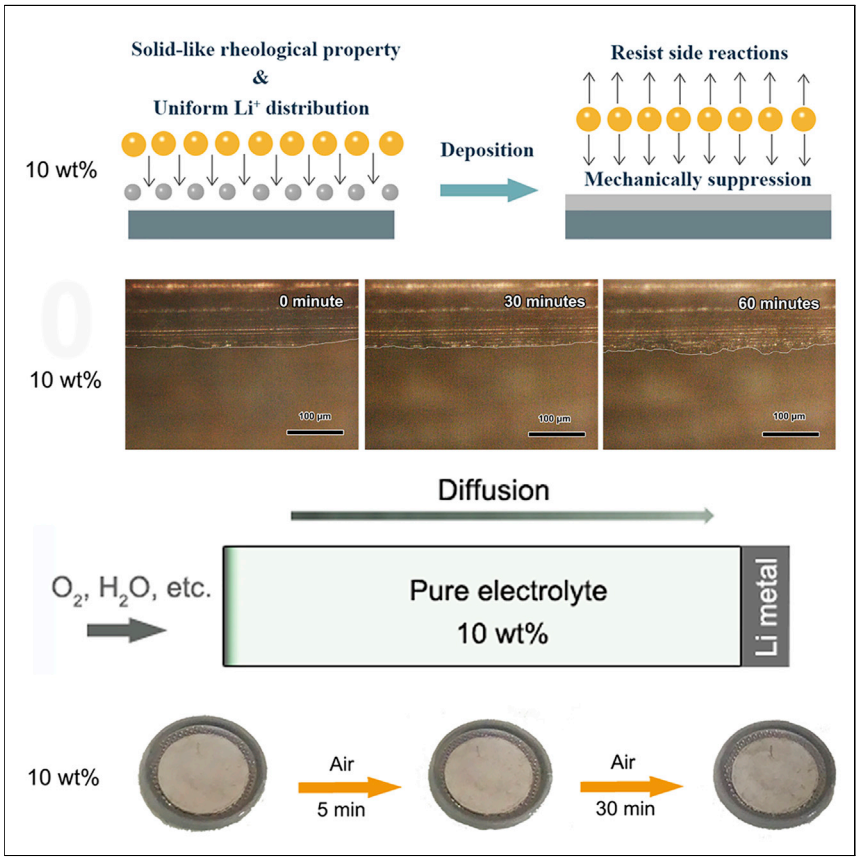

An electrolyte regulation strategy via *in situ* coupling of $CF_3SO_3^-$ and hydrophobic silica colloidal nanoparticles through electrostatic interaction is achieved. The seed crystal effect as well as anion-fixed and solid-like rheological properties can effectively prevent dendrites. The lower diffusion coefficient and hydrophobic property of nanosilica can lead to nearly 980-fold anticorrosion results. Consequently, the symmetrical batteries display 700 h of life with 30 mV overpotential and 45-fold lower R_{SEI}. Moreover, a 550-cycle anodic life is achieved in Li-O_2 batteries with 10 wt % HSCE.

Demonstrate
Proof-of-concept of performance with intended application/response

Yue Yu, Xin-Bo Zhang

xbzhang@ciac.ac.cn

HIGHLIGHTS

$CF_3SO_3^-$ *in situ* coupling with nanosilica via electrostatic interaction

Dendrite-free morphology and stable SEI film were obtained

Lower diffusion coefficient leads to a 980-fold better anticorrosion effect

Li-O_2 batteries with 10 wt % HSCE achieve 550 cycles of anodic life

Yu & Zhang, Matter 1, 881–892
October 2, 2019
https://doi.org/10.1016/j.matt.2019.06.002

Matter

CellPress

Article

In Situ Coupling of Colloidal Silica and Li Salt Anion toward Stable Li Anode for Long-Cycle-Life Li-O_2 Batteries

Yue Yu[1,2] and Xin-Bo Zhang[1,3,*]

SUMMARY

Lithium-oxygen (Li-O_2) batteries are promising next-generation batteries owing to their ultrahigh theoretical energy density. However, Li metal anodes in Li-O_2 batteries are still plagued by uncontrollable dendrite growth and serious parasitic reactions. Herein, we report an electrolyte regulation strategy via *in situ* coupling of $CF_3SO_3^-$ and hydrophobic silica colloidal nanoparticle through electrostatic interaction. With the assistance of the seed crystal effect and the solid-like rheological properties, 10 wt % hydrophobic silica colloid electrolyte (HSCE) enables the dendrite-free morphology of Li deposition and helps form a stable solid-electrolyte interface, which can reduce the impedance by about 45-fold after long-term cycling. Moreover, 10 wt % HSCE with a lower diffusion coefficient can achieve a 980-fold better anticorrosion effect than 0 wt % HSCE. Consequently, the 10 wt % HSCE batteries exhibit a stable plating/stripping process (30 mV in overpotential up to 700 h) and a good anodic cycle life in Li-O_2 batteries (550 cycles).

INTRODUCTION

With the rapid development and expanding demand of novel electric transportation and grid-scale power storage, traditional lithium-ion (Li-ion) batteries cannot satisfy the demand of such large-scale electricity consumption.[1–4] Rechargeable aprotic lithium-oxygen (Li-O_2) batteries have become burgeoning candidates because of their ultrahigh theoretical energy density of 3,500 Wh kg^{-1}, which is about 10-fold higher than that of Li-ion batteries.[5–7] Lithium metal as anode is one of the key factors in obtaining such high specific capacity thanks to its lowest electrochemical potential (−3.040 V versus standard hydrogen electrode) and high theoretical capacity (3,860 mAh g^{-1}).[8–10] However, the use of Li metal anode inevitably triggers serious safety issues because the dendrite growth of Li will pierce the separator and give rise to a short-circuit fire.[11–13] Furthermore, in sharp contrast to other Li metal-based batteries such as Li metal-ion battery and Li-S battery, the semi-open nature as well as the oxidizing environment of Li-O_2 batteries would result in more severe parasitic side reactions between Li anode and O_2 (dissolved in electrolyte), H_2O (generated from the decomposition of electrolyte), and other contaminants (e.g., discharge intermediate), which significantly hinders the development of Li-O_2 batteries.[14–16] Therefore, it is vital and urgent to open up a path to effectively protect the Li metal anode of Li-O_2 batteries.

Among many approaches proposed to protect the Li metal anode, electrolyte regulation is an effective approach to prevent dendrite growth and stabilize the electrode/electrolyte interface. Tuning of electrolyte composition (solvent, salt,

Progress and Potential

10 wt % hydrophobic silica colloid electrolyte (HSCE) is proposed to protect the Li metal anode from severe corrosion and irregular dendrite growth in Li-O_2 battery. This strategy simply couples the anion with nanosilica via electrostatic interaction to avoid the formation of a strong electrical field during the Li deposition process. The higher Li^+ transference number, uniform heterogeneous nucleation sites, and solid-like rheological properties can synergistically lead to uniform Li deposition. The symmetrical batteries with 10 wt % HSCE exhibit 30 mV overpotential until 700 h and nearly 45-fold lower resistance of SEI film (R_{SEI}). Furthermore, the low diffusion coefficient and hydrophobic property of silica lead to a 980-fold better anticorrosion effect in Li-O_2 batteries and 550 cycles of anodic life. It is worth noting that this comprehensive and effective protection strategy can spark more inspiration in alkali metal-O_2/air batteries, which is of great importance in promoting future energy development.

and additive) is a usual method to protect Li metal anode, whereas achieving good compatibility between the new electrolyte and electrodes is always challenging.[16–18] Very recently, the superconcentrated electrolyte has become a very important research subject due to its good dendrite-prevention effect.[19–21] However, more efforts should be devoted to further improve the wettability and decrease the cost of Li salt.[22] Nanostructured electrolyte with immobile anion can also effectively stabilize the Li/electrolyte interface and thus achieve a satisfactory electrochemical performance, but the current preparation process of such electrolyte is complex for practical application.[23,24] Therefore, it is paramount, while significantly challenging, to develop a facile and low-cost electrolyte regulation strategy to achieve a stable Li anode and Li/electrolyte interface.

Herein, as a proof-of-concept experiment, we propose and demonstrate an electrolyte regulation strategy by *in situ* coupling of $CF_3SO_3^-$ on the hydrophobic silica colloidal particles via electrostatic interactions. Unexpectedly, thanks to the seed crystal effect of the silica colloid particle and the solid-like rheological properties, the resultant hydrophobic silica colloid electrolyte (HSCE) results in a much smoother dendrite-free morphology and also behaves at greatly reduced impedance (about 45-fold lower after long cycling) due to a stable solid-electrolyte interface (SEI) film. Furthermore, the serious corrosion from O_2, H_2O, and other contaminants in Li-O_2 batteries can be effectively alleviated by 980-fold due to the low diffusion coefficient and the hydrophobic property of silica. More importantly, the 10 wt % HSCE endows the symmetrical batteries with a very low overpotential (30 mV) for up to 700 h and, especially, a stable anodic cycling of Li-O_2 batteries for up to 550 cycles.

RESULTS AND DISCUSSION

The commercial silica nanoparticles used here display a diameter of between 7 and 40 nm according to transmission electron microscopy images (Figure S1) and an excellent hydrophobic property verified by the contact angle test (Figure 1A). 10 wt % HSCE was obtained by homogeneously dispersing the hydrophobic nanosilica into the electrolyte (1 M $LiCF_3SO_3$ in tetraethylene glycol dimethyl ether) via a facial ultrasonic dispersion method. As the optical images in Figures 1B and S2 show, the as-obtained translucent electrolyte exhibits a clear Tyndall effect even after storing for 6 months, verifying a satisfactory thermodynamic stability of 10 wt % HSCE. Rheological measurement of 10 wt % HSCE displays a higher value of G' (storage modulus) than G'' (loss modulus) (Figure 1C), indicating solid-like rheological properties for the potential ability to suppress dendrite growth.[25,26]

The viscosity tests results are displayed in Figure 1D to assist in illustrating the contaminant prevention effect according to the Stokes-Einstein equation (Equation 1), where D is the diffusion constant, r is the radius of the particle, η is the viscosity of electrolyte, k_B is the Boltzmann constant, and T is the absolute temperature.[27]

$$D = \frac{k_B T}{6\pi\eta r}. \quad \text{(Equation 1)}$$

The diffusion coefficient of the corrosion (H_2O, O_2, and discharge intermediates) from the cathode side is inversely proportional to the viscosity of electrolyte. As Figure 1E shows, the viscosity of 10 wt % HSCE is about 980-fold higher than that of 0 wt % HSCE. In other words, the amount of corrosiveness in 10 wt % HSCE

[1]State Key Laboratory of Rare Earth Resource Utilization, Changchun Institute of Applied Chemistry, Chinese Academy of Sciences, Changchun 130022, P.R. China

[2]University of Science and Technology of China, Hefei 230026, P.R. China

[3]Lead Contact

*Correspondence: xbzhang@ciac.ac.cn

https://doi.org/10.1016/j.matt.2019.06.002

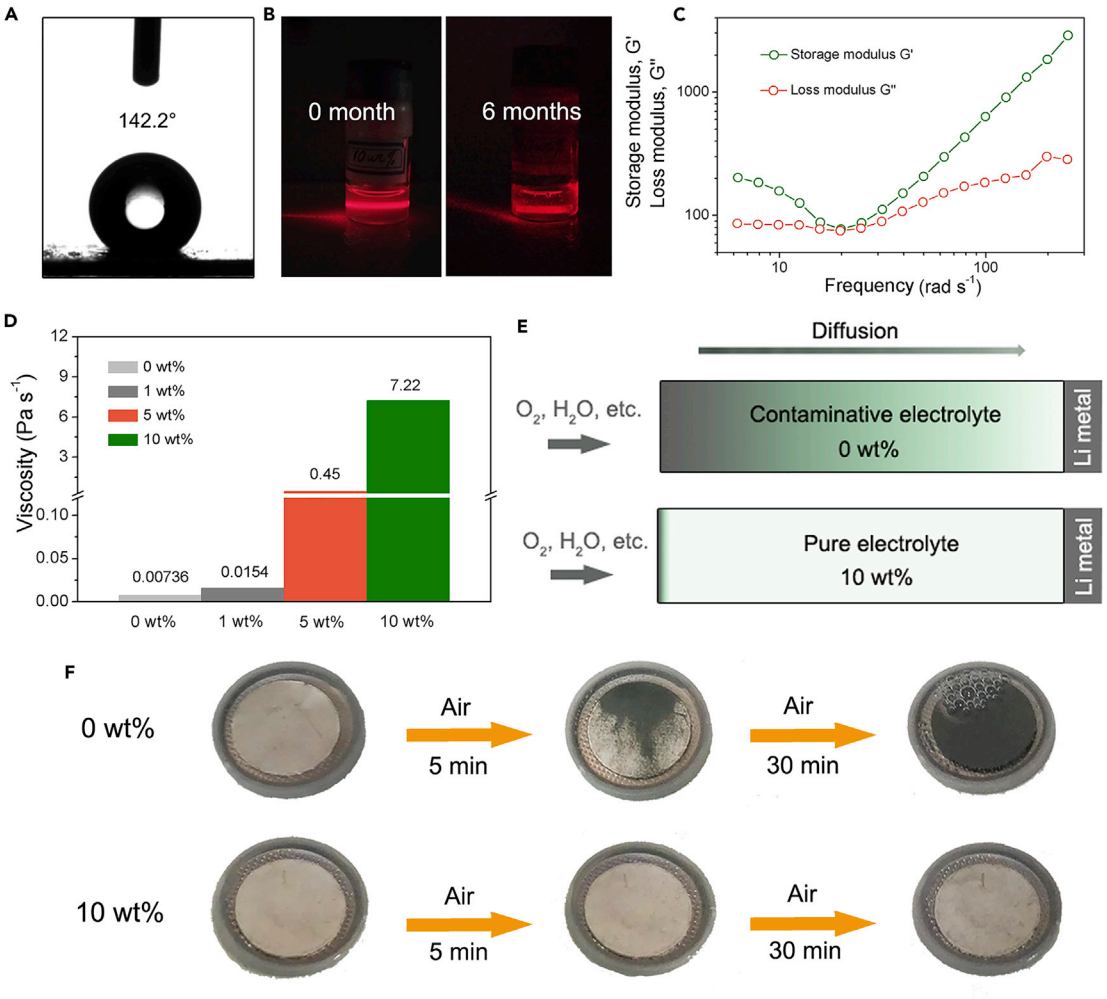

Figure 1. Characterization of 10 wt % HSCE

(A) H_2O contact angle image of hydrophobic silica nanoparticles.

(B) Tyndall effect images of 10 wt % HSCE before and after storing for 6 months.

(C) Storage modulus *G′* and loss modulus *G″* of 10 wt % HSCE.

(D) Viscosity of different kinds of electrolytes under the same shear rate.

(E) Schematic of the anticorrosion effect of different kinds of electrolytes.

(F) Optical images of the Li metal soaking in 0 wt % HSCE and 10 wt % HSCE exposed to air after 0 min, 5 min, and 30 min.

passing through per unit area in per unit time is about 980-fold lower than that in 0 wt % HSCE. Despite high viscosity, 10 wt % HSCE can also achieve satisfactory conductivity (Figure S4) and a good wettability (Figure S5), which is prerequisite to obtaining good electrochemical performance. To confirm the anticorrosion effect, we soaked two groups of Li sheets in 0 wt % and 10 wt % HSCE respectively and then exposed them to ambient air (relative humidity = 45%–50%). As Figure 1F presents, after being placed in ambient air just for 5 min, the color of Li sheet soaked in 0 wt % HSCE turns silver to black due to the uncontrollable side reactions with the contaminant in air. After 30 min, multiple bubbles derived from the drastic parasitic reactions between Li and water in air can be observed. In sharp contrast, the surface of the Li sheet soaked in 10 wt % HSCE still remains smooth and shiny even after 30 min, proving the excellent anticorrosion protection effect of this colloid electrolyte.

According to the Fajans rule, the silica colloid particles are prone to adsorbing the ions which have the same properties as SiO_2.[28] Also, the weak solvation of anion can also assist $CF_3SO_3^-$ adsorption because the Li^+ ion, which is coordinated to four oxygen atoms within G4 molecules, is difficult to adsorb on the surface of colloid nucleus.[29] We conjectured that $CF_3SO_3^-$ is adsorbed on the SiO_2 surface as Figure 2A demonstrates. This conjecture is also consistent with the experimental results of Li^+ transference number test. As Figures S7 and S8 show, higher Li^+ transport number of 10 wt % HSCE (t_{Li+} = 0.78) than that of 0 wt % HSCE (t_{Li+} = 0.61) indicates the fixation effect of the $CF_3SO_3^-$ caused by the adsorption of colloidal particles.[30] As Equation 2 shows, τ_s (Sand's time) is the time corresponding to the drop in the anion concentration at Li/electrode interface to zero,[31,32]

$$\tau_s = \frac{\pi D (nF)^2 C_0^2}{4 J^2 t_a^2}, \qquad \text{(Equation 2)}$$

where D is the ambipolar diffusivity, n is the valence of the salt, F is Faraday's constant, C_0 is the bulk concentration, J is the applied current density, and t_a is the anion transference number. According to the space-charge theory proposed by Chazalviel, the higher t_a can effectively restrain the large electric field caused by the anion depletion, which can alleviate the ramified dendrite growth.[33,34] Besides, equally distributed silica colloid particles can be the seed crystal to lead to stable Li deposition due to the heterogeneous nucleation mechanism, thus finally enabling dendrite-free Li deposition.(Figure S9)[35] The dendrite-prevention effect of 10 wt % HSCE is clearly summarized in Figure 2B.

In situ optical microscopy was used to intuitionally verify the dendrite-suppression effect of 10 wt % HSCE. Figures 2C–2H show the cross-section of Li metal anodes running in 0 and 10 wt % HSCE. It can be observed that the serious uneven dendrites grow continuously on the surface of the Li in the 0 wt % HSCE during the tests (Figures 2C–2E). In comparison, the Li morphology in 10 wt % HSCE maintains smooth during the deposition process, which clearly reveals the dendrite-prevention effect of 10 wt % HSCE electrolyte (Figures 2F–2H). To reveal the role of different electrolytes on Li deposition behavior in more detail, the scanning electron microscopy (SEM) images of Li plating morphology using 0 wt % and 10 wt % HSCE are displayed in Figures 2I and 2J. The Li deposition shows an obvious irregular dendrite growth in 0 wt % HSCE (Figure 2I), while that in 10 wt % HSCE exhibits a relatively much smoother surface (Figure 2J), indicating the 10 wt % HSCE has a good dendrite-suppression effect.

To investigate the stability of Li/electrolyte interface, we tested the Li/Li symmetrical cells in 0 wt % and 10 wt % HSCE. In Figures 3A–3D, at the beginning of the plating and stripping process both of the cells show similar overpotential because the side reaction production and broken SEI film do not accumulate sufficiently on the Li surface to obviously affect the overpotential. With the batteries running, the cells with 0 wt % HSCE exhibit an ultrahigh overpotential that reaches up to 5 V after 90 cycles. On the contrary, the cells with 10 wt % HSCE display a much lower hysteresis (30 mV) and more stable cycles even until 700 h. The voltage hysteresis evolution comparison between the two groups of batteries at different cycles also clearly demonstrates the improvement of overpotential and cycle life with 10 wt % HSCE (Figure 3E). Even at a higher current density, the symmetrical batteries with 10 wt % HSCE still exhibit longer, more stable, and lower overpotential cycling as shown in Figure S11.

The stability of Li/electrolyte interface was further illustrated by the electrochemical impedance spectroscopy (EIS). First, EIS analysis was performed before and after

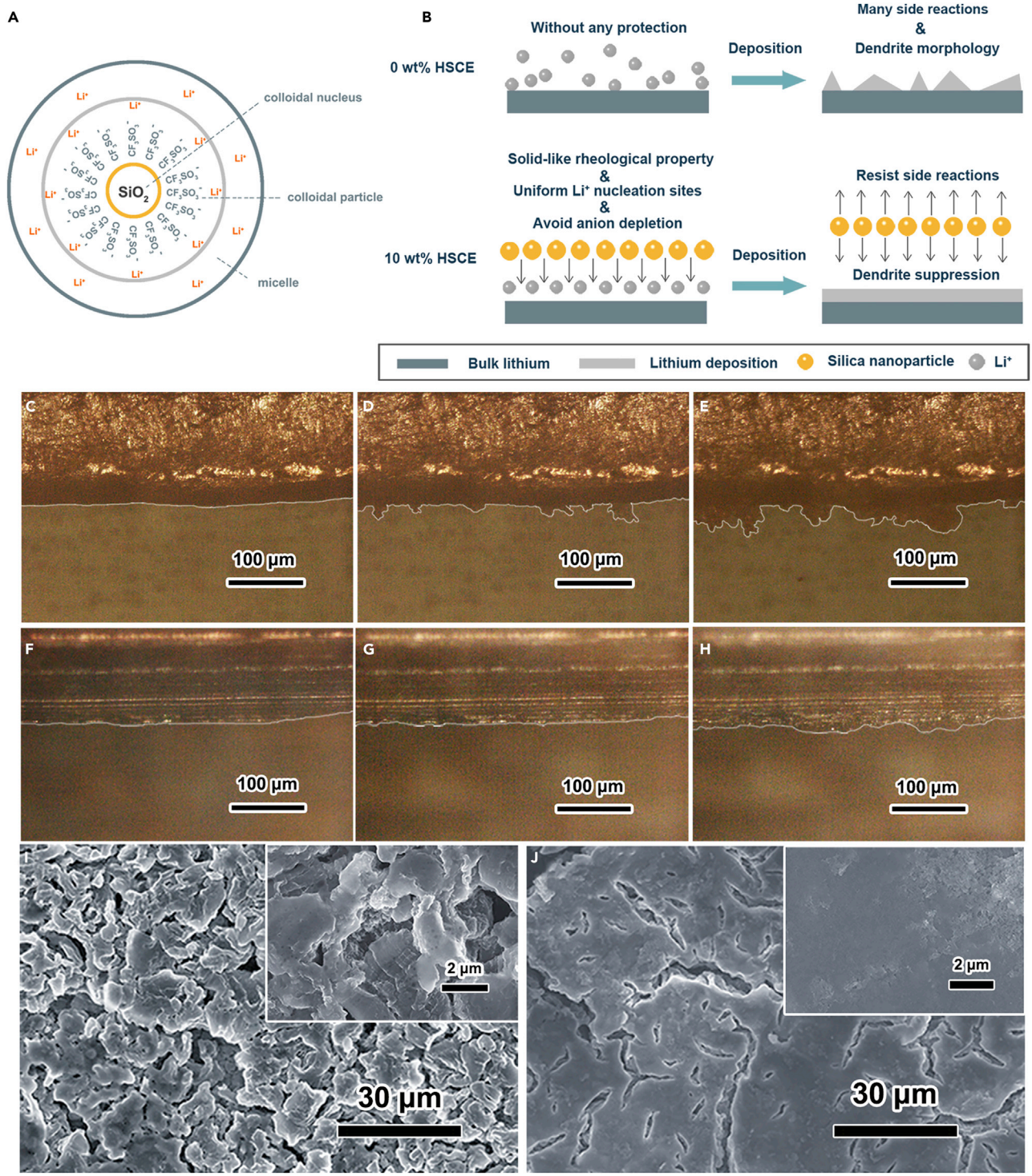

Figure 2. Deposition Behavior of Lithium in Different Electrolytes

(A) Schematic of the ion-adsorption condition of micelle in 10 wt % HSCE.

(B) Schematic of the dendrite-suppression effect during Li deposition process in 0 wt % and 10 wt % HSCE.

(C–H) *In situ* optical microscopy images of Li deposition in 0 wt % HSCE for (C) 0 min, (D) 30 min, and (E) 60 min. *In situ* optical microscopy images of Li deposition in 10 wt % HSCE for (F) 0 min, (G) 30 min, and (H) 60 min.

(I–J) Low-magnification SEM images of Li deposition morphology in 0 wt % HSCE (I) and 10 wt % HSCE (J); insets are the high-magnification images of Li deposition morphology in corresponding electrolyte.

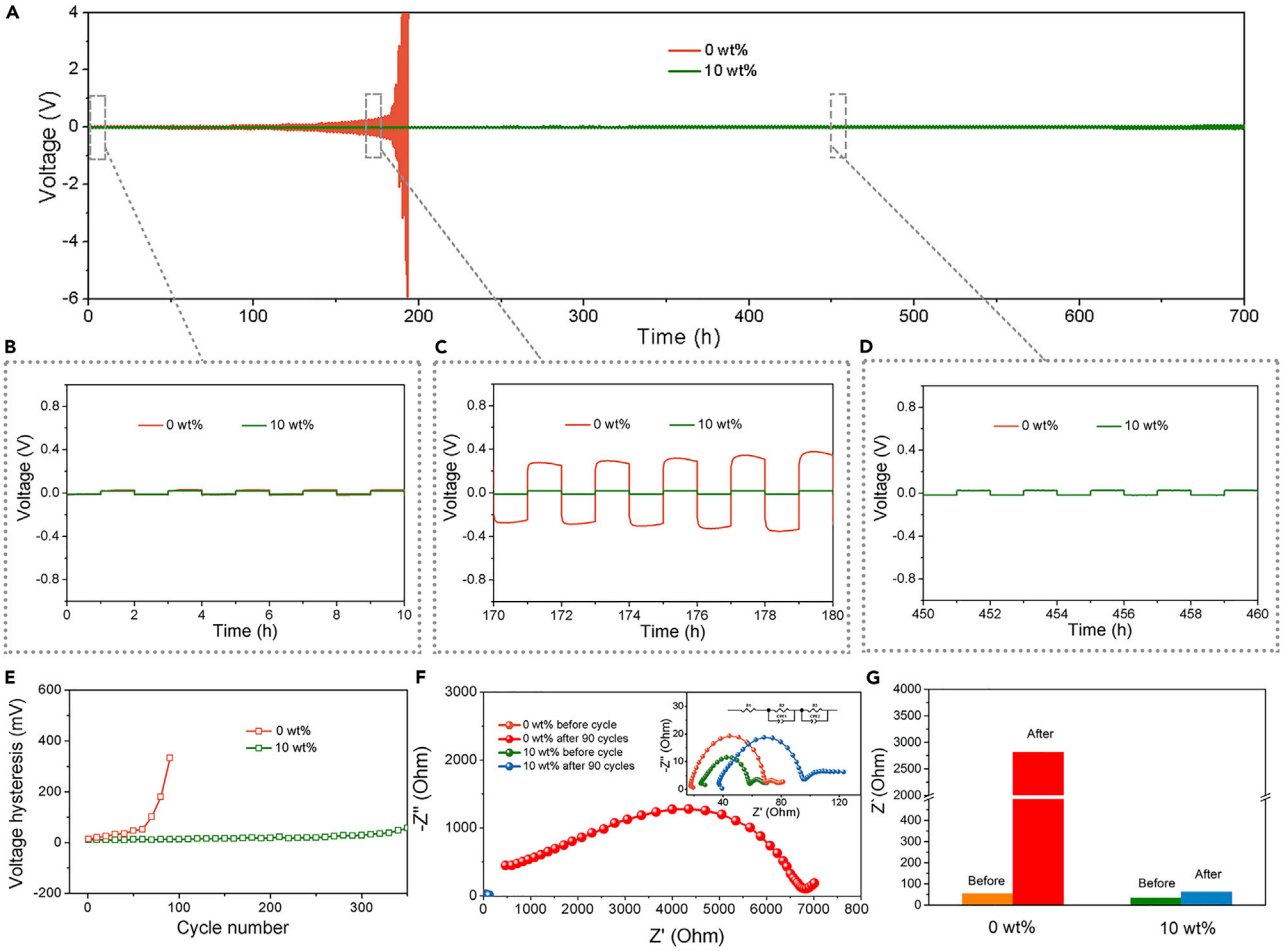

Figure 3. Electrochemical Performance of Symmetrical Batteries with Different Electrolytes

(A–D) Electrochemical performance of Li/Li symmetrical batteries with 0 wt % and 10 wt % HSCE at a current density of 0.1 mA cm^{-2} (each plating and stripping time is 1 h) (A), and zoomed segments of the voltage profiles (B) between 0 and 10 h, (C) between 170 and 180 h, and (D) between 450 and 460 h.

(E) Corresponding voltage hysteresis curves of Li/Li symmetrical batteries.

(F and G) Nyquist plot of the impedance spectra of symmetrical batteries with 0 wt % and 10 wt % HSCE before and after long-term cycles (F) and corresponding R_{SEI} value bar graph with 0 wt % HSCE and 10 wt % HSCE (G).

long-term storage, as Figure S13 displays. After storing for around 20 days, much less impedance increase can be observed in 10 wt % HSCE batteries than that in 0 wt % HSCE, indicating that the 10 wt % HSCE can minimize the resistance of SEI film (R_{SEI}) between Li metal anode and electrolyte.[36,37] It can be reasoned that this SEI film can be strong enough to effectively isolate Li metal anode from the electrolyte corrosion. Without the protection of colloid electrolyte, the side reaction products will accumulate sufficiently on the Li surface to increase the R_{SEI}. We further tested the EIS of batteries after different cycles. In Figures 3F and 3G, after long-time cycling the R_{SEI} in 0 wt % HSCE considerably increase by 52-fold while that in 10 wt % HSCE only changed a little, consistent with the overpotential change of symmetrical curves. The ultrahigh impedance indicated that the unstable SEI film repeatedly breaks and reforms, thus finally becoming too thick to conduct ions and killing the batteries.[9,38] These results sufficiently illustrate that the 10 wt % HSCE can build a stable Li/electrolyte interface and restrain the nonlimiting SEI formation and breaking process as well as the continuous side reactions.

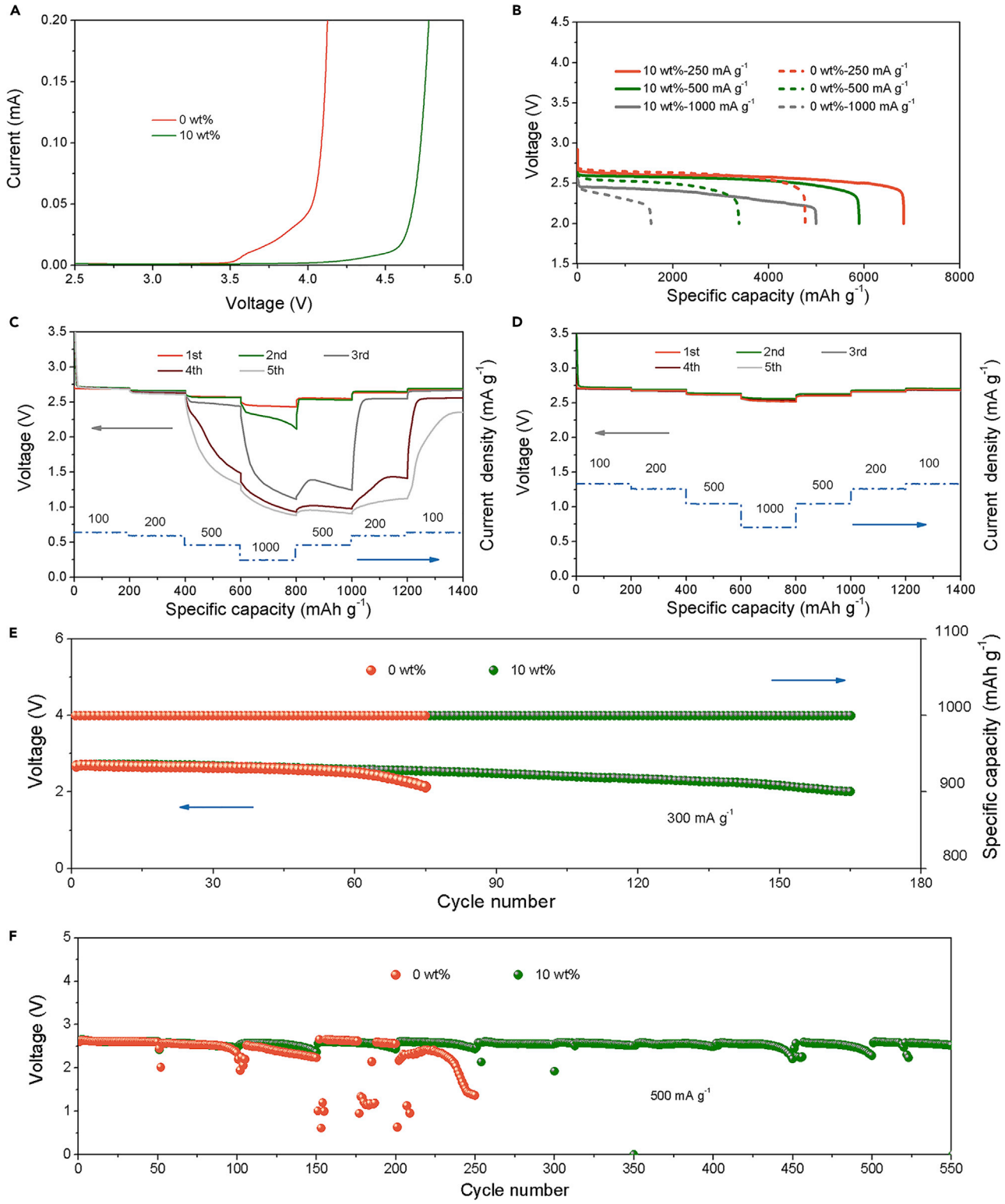

Figure 4. Electrochemical Performance of Li-O_2 Batteries with Different Electrolytes

(A) LSV curves of 0 wt % HSCE and 10 wt % HSCE.

(B) Discharge curves of Li-O_2 batteries with 0 wt % HSCE and 10 wt % HSCE under different current densities.

(C) Rate performance at different cycles of Li-O_2 batteries with 0 wt % HSCE.

Figure 4. *Continued*

(D) Rate performance at different cycles of Li-O_2 batteries with 10 wt % HSCE.

(E) Cycle performance of Li-O_2 batteries with 0 wt % HSCE and 10 wt % HSCE with a specific capacity of 1,000 mAh g^{-1}.

(F) Anodic cycle life of Li-O_2 batteries with 0 wt % HSCE and 10 wt % HSCE.

Encouraged by the dendrite-free deposition and the stabilized Li/electrolyte interface obtained from the 10 wt % HSCE, the Li-O_2 batteries using 10 wt % HSCE were assembled. The electrochemical stability of the 10 wt % HSCE, the electrochemical stability window is demonstrated and verified in Figure 4A. With the increasing content of the silica, the 10 wt % HSCE behaves in a much wider electrolyte window, indicating that the addition of silica can enhance the electrochemical stability of electrolyte. The redox reactions of Li-O_2 batteries with 10 wt % HSCE are demonstrated by the cyclic voltammetry tests in Figure S16. The curves exhibit the typical oxidation and reduction peaks of the Li-O_2 batteries reported in previous literature, which indicates that the 10 wt % HSCE does not affect the main reactions in the Li-O_2 batteries.[39,40] Figure 4B displays the full discharge-charge curves of Li-O_2 batteries with different kinds of electrolytes at various current densities. The Li-O_2 batteries with 10 wt % HSCE always exhibit a higher capacity than those with 0 wt % HSCE at different current densities, especially at a high current density of 1,000 mA g^{-1}. Furthermore, the rate performance of the Li-O_2 batteries was tested, the results of which are shown in Figures 4C and 4D. Although the discharge voltage of the batteries with 0 wt % HSCE is a little higher than that with 10 wt % HSCE at the beginning of the cycling process, in the following cycles a much lower and more unstable voltage plateau is observed at each current density, especially at high current density of 1,000 mA g^{-1}, while that of 10 wt % HSCE is very stable. Another improvement of the Li-O_2 batteries with 10 wt % HSCE is its cycling life. As seen in Figure 4E, the Li-O_2 batteries with 10 wt % HSCE can run for 168 cycles before the voltage drops to 2.0 V. By contrast, the batteries with 0 wt % HSCE can only operate over 77 cycles under the same circumstances. Anodic cycle life of Li-O_2 batteries also benefits from the excellent protection effect of the Li metal anodes. As shown in Figure 4F, rebuilt batteries were assembled by replacing the cathode after every 50 cycles to check the reversibility of anodes. Li-O_2 batteries with 0 wt % HSCE can only cycle for 250 cycles at a current density of 500 mA g^{-1} before the anode fails. In the opposite case, Li-O_2 batteries with 10 wt % HSCE display a longer cycle life up to 550 cycles, which is attributed to the effective anticorrosion effect resulting from the 10 wt % HSCE.

In Li-O_2 batteries, the more important and challenging anode anticorrosion effect of 10 wt % HSCE is demonstrated as follows. X-ray diffraction (XRD) was chosen as a direct tool to reveal the degree of corrosion of Li because the intensity of the LiOH peaks can indicate the corrosion extent.[41] In Figures 5B and 5C, the Li metal anodes in Li-O_2 batteries with 0 wt % HSCE after 50 cycles exhibit much higher LiOH peak intensity than that of 10 wt % HSCE, which confirms a much more serious corrosion of the Li metal anodes without protection. The corresponding morphology corrosion evolution is illustrated in Figures 5D–5G. After 20 cycles, the surface morphology of Li metal anode with 0 wt % HSCE is much rougher than that with 10 wt % HSCE. After 50 cycles, deep crevices form on the surface of the Li metal anode in 0 wt % HSCE while the Li anode in 10 wt % HSCE displays a much flatter surface, verifying the significant anticorrosion effect of 10 wt % HSCE.

To further study the discharge products of Li-O_2 batteries with 10 wt % HSCE, we conducted SEM to investigate the morphology of air cathode after discharging

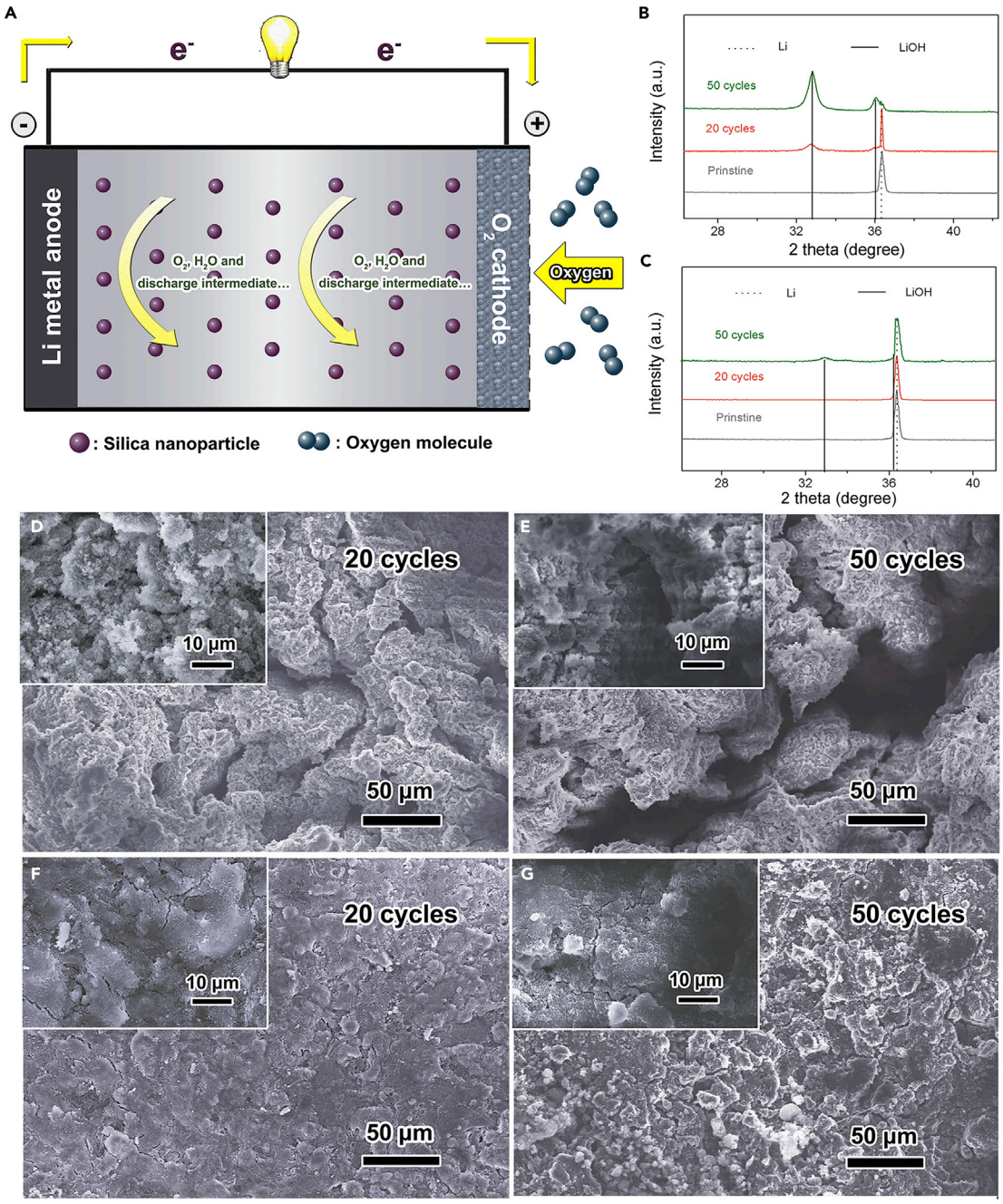

Figure 5. Surface Corrosion Condition of Lithium after Cycling in Li-O_2 Batteries with Different Electrolytes

(A) Schematic of the mechanism of the anticorrosion effect of 10 wt % HSCE in Li-O_2 batteries.

(B and C) XRD patterns of the Li metal that operated in Li-O_2 batteries with 0 wt % HSCE (B) and 10 wt % HSCE (C) after different cycles.

(D–G) SEM images of Li metal anode surface morphology operated in Li-O_2 batteries with 0 wt % HSCE after (D) 20 cycles and (E) 50 cycles. SEM images of Li metal anode surface morphology operated in Li-O_2 batteries with 10 wt % HSCE after (F) 20 cycles and (G) 50 cycles.

and charging. As Figures S20 and S21 show, the discharge products in Li-O_2 batteries display an increased diameter of toroid-shape Li_2O_2 with increasing silica content. We speculate that the silica, which has a high specific surface area (Figure S22), may adsorb the polar molecular LiO_2^- to promote the solution-growth process and assist greater Li_2O_2 formation.[6,42] Cathode reversibility was

also tested in the Li-O_2 batteries with 10 wt % HSCE electrolyte (Figures S23 and S24). The SEM images reveal that the toroid-shape Li_2O_2 formed after the discharge process can be decomposed after the charge process. The aforementioned results of electrochemical performances and properties of the cathode indicate that the 10 wt % HSCE has good compatibility between electrolyte and electrode.

Conclusion

In summary, a facile and low-cost 10 wt % HSCE is prepared to effectively protect the Li metal anodes from severe corrosion and irregular dendrite growth in Li-O_2 batteries. Three aspects make 10 wt % HSCE an innovative and effective method. (1) Compared with complex preparation steps applied in the nanostructured electrolyte to fix the anion, 10 wt % HSCE instinctively facilitates the adsorption of the $CF_3SO_3^-$ on the surface of the colloid nucleus and avoids the formation of a strong electrical field caused by anion depletion. Additionally, the low-cost raw materials of 10 wt % HSCE solve the exorbitant price challenge of superconcentrated electrolyte without sacrificing performance, while 10 wt % HSCE overcomes the incompatibility between electrode and electrolyte, which always disturbs batteries using electrolyte regulation methods. (2) The higher Li-ion transference number, the uniform heterogeneous nucleation sites, and solid-like rheological properties can synergistically lead to a dendrite-free Li deposition. Moreover, 10 wt % HSCE can effectively stabilize the Li/electrolyte interface and prevent the SEI film from repeated damage and formation. The symmetrical batteries with 10 wt % HSCE exhibit a more stable and longer cycle life (30 mV in overpotential up to 700 h) as well as a nearly 45-fold lower R_{SEI}. (3) With the help of low diffusion coefficient and the hydrophobic property of silica, 10 wt % HSCE produces a 980-fold better anticorrosion effect to defend O_2, H_2O, and other contaminants in Li-O_2 batteries. The Li metal anode in Li-O_2 batteries displays much less corrosion morphology and a much longer anodic cycle life (550 cycles). Thus, this strategy can effectively reduce the dendrite growth and serious side reactions, thus leading to a satisfactory electrochemical performance. Gazing to the future, this comprehensive and effective protection strategy can spark more inspiration in Li-air battery and Na-air battery research.

EXPERIMENTAL PROCEDURES

Full details of experimental procedures are provided in Supplemental Information.

SUPPLEMENTAL INFORMATION

Supplemental Information can be found online at https://doi.org/10.1016/j.matt.2019.06.002.

ACKNOWLEDGMENTS

This work was financially supported by the National Natural Science Foundation of China (21725103), National Key R&D Program of China (2016YFB0100100), and Jilin Province Science and Technology Development Program (20160101289JC).

AUTHOR CONTRIBUTIONS

Y.Y and X.-B.Z. designed this work. Y.Y conducted the electrochemical experiment. Y.Y. and X.-B.Z. analyzed the experimental data and wrote the paper.

DECLARATION OF INTERESTS

The authors declare no competing interests.

Received: December 30, 2018
Revised: April 4, 2019
Accepted: June 3, 2019
Published: August 28, 2019

REFERENCES

1. Dunn, B., Kamath, H., and Tarascon, J.-M. (2011). Electrical energy storage for the grid: a battery of choices. Science *334*, 928–935.

2. Bruce, P.G., Freunberger, S.A., Hardwick, L.J., and Tarascon, J.-M. (2011). Li-O_2 and Li-S batteries with high energy storage. Nat. Mater. *11*, 19–29.

3. Chan, C.K., Peng, H., Liu, G., McIlwrath, K., Zhang, X.F., Huggins, R.A., and Cui, Y. (2008). High-performance lithium battery anodes using silicon nanowires. Nat. Nanotechnol. *3*, 31–35.

4. Armand, M., and Tarascon, J.-M. (2008). Building better batteries. Nature *451*, 652–657.

5. Aurbach, D., McCloskey, B.D., Nazar, L.F., and Bruce, P.G. (2016). Advances in understanding mechanisms underpinning lithium–air batteries. Nat. Energy *1*, 16128.

6. Lyu, Z., Zhou, Y., Dai, W., Cui, X., Lai, M., Wang, L., Huo, F., Huang, W., Hu, Z., and Chen, W. (2017). Recent advances in understanding of the mechanism and control of Li_2O_2 formation in aprotic Li-O_2 batteries. Chem. Soc. Rev. *46*, 6046–6072.

7. Ogasawara, T., Débart, A., Holzapfel, M., Novék, P., and Bruce, P.G. (2006). Rechargeable Li_2O_2 electrode for lithium batteries. J. Am. Chem. Soc. *128*, 1390–1393.

8. Gao, Y., Zhao, Y., Li, Y.C., Huang, Q., Mallouk, T.E., and Wang, D. (2017). Interfacial chemistry regulation via a skin-grafting strategy enables high-performance lithium-metal batteries. J. Am. Chem. Soc. *139*, 15288–15291.

9. Lin, D., Liu, Y., Chen, W., Zhou, G., Liu, K., Dunn, B., and Cui, Y. (2017). Conformal lithium fluoride protection layer on three-dimensional lithium by nonhazardous gaseous reagent freon. Nano Lett. *17*, 3731–3737.

10. Pang, Q., Liang, X., Shyamsunder, A., and Nazar, L.F. (2017). An in vivo formed solid electrolyte surface layer enables stable plating of Li metal. Joule *1*, 871–886.

11. Cheng, X.B., Yan, C., Chen, X., Guan, C., Huang, J.Q., Peng, H.J., Zhang, R., Yang, S.T., and Zhang, Q. (2017). Implantable solid electrolyte interphase in lithium-metal batteries. Chem *2*, 258–270.

12. Liu, F., Xiao, Q., Wu, H.B., Shen, L., Xu, D., Cai, M., and Lu, Y. (2018). Fabrication of hybrid silicate coatings by a simple vapor deposition method for lithium metal anodes. Adv. Energy Mater. *8*, 1701744.

13. Li, N.W., Shi, Y., Yin, Y.X., Zeng, X.X., Li, J.Y., Li, C.J., Wan, L.J., Wen, R., and Guo, Y.G. (2018). A flexible solid electrolyte interphase layer for long-life lithium metal anodes. Angew. Chem. Int. Ed. *57*, 1505–1509.

14. Liu, Q.C., Xu, J.J., Yuan, S., Chang, Z.W., Xu, D., Yin, Y.B., Li, L., Zhong, H.X., Jiang, Y.S., Yan, J.M., and Zhang, X.B. (2015). Artificial protection film on lithium metal anode toward long-cycle-life lithium-oxygen batteries. Adv. Mater. *27*, 5241–5247.

15. Xu, J.J., Liu, Q.C., Yu, Y., Wang, J., Yan, J.M., and Zhang, X.B. (2017). In situ construction of stable tissue-directed/reinforced bifunctional separator/protection film on lithium anode for lithium-oxygen batteries. Adv. Mater. *29*, 1606552.

16. Choudhury, S., Wan, C.T., Sadat, W.I.A., Tu, Z.Y., Lau, S., Zachman, M.J., Kourkoutis, L.F., and Archer, L.A. (2017). Designer interphases for the lithium-oxygen electrochemical cell. Sci. Adv. *3*, e1602809.

17. Eshetu, G.G., Judez, X., Li, C.M., Bondarchuk, A., RodriguezMartinez, L.M., Zhang, H., and Armand, M. (2017). Lithium azide as an electrolyte additive for all-solid-state lithium–sulfur batteries. Angew. Chem. Int. Ed. *56*, 15368–15372.

18. Tong, B., Huang, J., Zhou, Z., and Peng, Z. (2018). The salt matters: enhanced reversibility of Li-O_2 batteries with a Li[$(CF_3SO_2)(n\text{-}C_4F_9SO_2)$N]-based electrolyte. Adv. Mater. *30*, 1704841.

19. Ren, X., Chen, S., Lee, H., Mei, D., Engelhard, M.H., Burton, S.D., Zhao, W., Zheng, J., Li, Q., Ding, M.S., et al. (2018). Localized high-concentration sulfone electrolytes for high-efficiency lithium-metal batteries. Chem *4*, 1877–1892.

20. Suo, L., Hu, Y.S., Li, H., Armand, M., and Chen, L. (2013). A new class of Solvent-in-Salt electrolyte for high-energy rechargeable metallic lithium batteries. Nat. Commun. *4*, 1481.

21. Suo, L.M., Borodin, O., Gao, T., Olguin, M., Ho, J., Fan, X.L., Luo, C., Wang, C.S., and Xu, K. (2015). "Water-in-salt" electrolyte enables high-voltage aqueous lithium-ion chemistries. Science *350*, 938–943.

22. Cheng, X.B., Zhang, R., Zhao, C.Z., and Zhang, Q. (2017). Toward safe lithium metal anode in rechargeable batteries: a review. Chem. Rev. *117*, 10403–10473.

23. Lu, Y., Das, S.K., Moganty, S.S., and Archer, L.A. (2012). Ionic liquid-nanoparticle hybrid electrolytes and their application in secondary lithium-metal batteries. Adv. Mater. *24*, 4430–4435.

24. Lu, Y., Korf, K., Kambe, Y., Tu, Z., and Archer, L.A. (2014). Ionic-liquid-nanoparticle hybrid electrolytes: applications in lithium metal batteries. Angew. Chem. Int. Ed. *53*, 488–492.

25. Ueno, K., Hata, K., Katakabe, T., Kondoh, M., and Watanabe, M. (2008). Nanocomposite ion gels based on silica nanoparticles and an ionic liquid: ionic transport, viscoelastic properties, and microstructure. J. Phy. Chem. B *112*, 9013–9019.

26. Moganty, S.S., Srivastava, S., Lu, Y., Schaefer, J.L., Rizvi, S.A., and Archer, L.A. (2012). Ionic liquid-tethered nanoparticle suspensions: a novel class of ionogels. Chem. Mater. *24*, 1386–1392.

27. Tuteja, A., and Mackay, M.E. (2007). Breakdown of the continuum Stokes-Einstein relation for nanoparticle diffusion. Nano Lett. *7*, 1276–1281.

28. Currin, B.L., Kennedy, R.M., Clarke, A.N., and Wilson, D.J. (1979). Electrical aspects of adsorbing colloid flotation. X. Pretreatments, multiple removals, interferences, and specific adsorption. Sep. Sci. Technol. *14*, 669–687.

29. Mandai, T., Yoshida, K., Tsuzuki, S., Nozawa, R., Masu, H., Ueno, K., Dokko, K., and Watanabe, M. (2015). Effect of ionic size on solvate stability of glyme-based solvate ionic liquids. J. Phys. Chem. B *119*, 1523–1534.

30. Fan, L., Wei, S., Li, S., Li, Q., and Lu, Y. (2018). Recent progress of the solid-state electrolytes for high-energy metal-based batteries. Adv. Energy Mater. *8*, 1702657.

31. Rosso, M., Brissot, C., Teyssot, A., Dollé, M., Sannier, L., Tarascon, J.-M., Bouchet, R., and Lascaud, S. (2006). Dendrite short-circuit and fuse effect on Li/polymer/Li cells. Electrochim. Acta *51*, 5334–5340.

32. Sand, H.J.S. (1901). III. On the concentration at the electrodes in a solution, with special reference to the liberation of hydrogen by electrolysis of a mixture of copper sulphate and sulphuric acid. London Edinburgh Dublin Philos. Mag. J. Sci. *1*, 45–79.

33. Fleury, V., Chazalviel, J.-N., Rosso, M., and Sapoval, B. (1990). The role of the anions in the growth speed of fractal electrodeposits. J. Electroanal. Chem. *290*, 249–255.

34. Chazalviel, J.N. (1990). Electrochemical aspects of the generation of ramified metallic electrodeposits. Phys. Rev. A *42*, 7355–7367.

35. Ely, D.R., and García, R.E. (2013). Heterogeneous nucleation and growth of lithium electrodeposits on negative electrodes. J. Electrochem. Soc. *160*, A662–A668.

36. Cheng, X.B., Zhao, M.Q., Chen, C., Pentecost, A., Maleski, K., Mathis, T., Zhang, X.Q., Zhang, Q., Jiang, J., and Gogotsi, Y. (2017). Nanodiamonds suppress the growth of lithium dendrites. Nat. Commun. *8*, 336.

37. Zhao, J., Liao, L., Shi, F., Lei, T., Chen, G., Pei, A., Sun, J., Yan, K., Zhou, G., Xie, J., et al. (2017). Surface fluorination of reactive battery anode materials for enhanced stability. J. Am. Chem. Soc. *139*, 11550–11558.

38. Wan, G., Guo, F., Li, H., Cao, Y., Ai, X., Qian, J., Li, Y., and Yang, H. (2018). Suppression of dendritic lithium growth by in situ formation of a chemically stable and mechanically strong solid electrolyte interphase. ACS Appl. Mater. Interfaces *10*, 593–601.

39. Li, F., Ohnishi, R., Yamada, Y., Kubota, J., Domen, K., Yamada, A., and Zhou, H. (2013). Carbon supported TiN nanoparticles: an efficient bifunctional catalyst for non-aqueous Li-O_2 batteries. Chem. Commun. *49*, 1175–1177.

40. Laoire, C.O., Mukerjee, S., Abraham, K.M., Plichta, E.J., and Hendrickson, M.A. (2010). Influence of nonaqueous solvents on the electrochemistry of oxygen in the rechargeable lithium–air battery. J. Phys. Chem. C *114*, 9178–9186.

41. Shui, J.L., Okasinski, J.S., Kenesei, P., Dobbs, H.A., Zhao, D., Almer, J.D., and Liu, D.J. (2013). Reversibility of anodic lithium in rechargeable lithium-oxygen batteries. Nat. Commun. *4*, 2255.

42. Yu, W., Wang, H., Hu, J., Yang, W., Qin, L., Liu, R., Li, B., Zhai, D., and Kang, F. (2018). Molecular sieve induced solution growth of Li_2O_2 in the Li-O_2 battery with largely enhanced discharge capacity. ACS Appl. Mater. Interfaces *10*, 7989–7995.